ELSEVIER

Physics of the Earth and Planetary Interiors 88 (1995) 211–221

PHYSICS OF THE EARTH AND PLANETARY INTERIORS

A description of metamorphic *PTt* paths with implications for low-*P* high-*T* metamorphism

Kurt Stüwe *, Mike Sandiford

Department of Geology and Geophysics, The University of Adelaide, Adelaide, SA 5005, Australia

Received 8 June 1993; revision accepted 11 August 1994

Abstract

The terms "clockwise" and "anticlockwise" are well entrenched in the metamorphic geology literature where they are used to describe, respectively, decompression or compression of rocks at and after the metamorphic temperature peak. Accordingly, we define the clockwiseness of a *PT* path, *C*, as the rate of pressure change at the temperature maximum, $C = \mathrm{d}P/\mathrm{d}t\,|_{T\max}$ and suggest that *C* may be used to characterise metamorphic *PT* paths. We illustrate this approach using a simple one-dimensional kinematic model with a prescribed strain-rate evolution and a thermal model in which the thermal evolution is governed by a cooling intrusion and we consider both the lithostatic and the deviatoric stress contributions to the pressure field. In a parallel paper we have shown that, because of the consideration of deviatoric stresses in this model, *PT* paths may vary from clockwise to anticlockwise, depending on distance form the intrusion and/or subtle changes of the assumptions of the strain-rate evolution. This result is important as it challenges many current interpretations of *PT* paths in particular those from the low-*P* high-*T* metamorphic environment. Here, we use the simple parameter *C* to investigate some of the governing controls on the shape variations of such paths.

1. Introduction

Metamorphic pressure–temperature time (*PTt*) paths are an important aid for the interpretation of metamorphic rocks. Paths may involve decompression after the metamorphic temperature peak (often termed "clockwise" paths), or isobaric cooling or compression during the cooling history (termed "anticlockwise" paths). In low-pressure, high-temperature (LPHT) terrains qualitatively different *PT* paths have been found in terrains with otherwise very similar metamorphic peak conditions and structural signatures (Harley, 1989) and paths of both shapes have even been found within the same terrain (Sisson and Hollister, 1988; Sisson et al., 1989; Yamamoto, 1992). In a recent contribution we have suggested that such observations may provide evidence for an important contribution of deviatoric stresses to the total pressure field with the proviso that thermodynamic pressure in deforming rock aggregates can be related to the mean stress. Consequently, the tectonic significance of *PT* paths remains extremely contentious (Stüwe and Sandiford, 1994). With this suggestion we appeal

* Corresponding author.

SSDI 0031-9201(94)02985-7

to some rehabilitation of the ideas of tectonic overpressure (see also Mancktelow, 1993). We were able to show that pressure changes of up to about 1 kbar may relate to changes in the deviatoric component of the stress field as governed by the interplay of temperature and strain-rate changes so that clockwise and anticlockwise *PT* paths may occur within the same LPHT terrain with their shape depending on the local magnitude of the deviatoric stress field. However, we did not explore the parameters that govern spatial variations in the shape of *PT* paths but rather focused on the geological application. In this paper we concentrate on details of the controls on shape of such paths with the aim to improve our understanding of how temperature and strain-rate changes in a continuously deforming medium may contribute to changes in the pressure field. In our approach we describe the shape of *PT* paths with only one parameter, their "clockwiseness", C. Analytical expressions for this clockwiseness are derived which may be used to investigate details of the likely *PT* paths that may arise for an assumed rheology, temperature and strain-rate evolution.

2. The clockwiseness of *PT* paths

Metamorphic rocks record, in general, only a portion of their *PT* evolution, namely a small section of the retrograde path following the metamorphic temperature peak, T_{max}. Many *PT* paths can therefore be characterised by the qualitative pressure change near the metamorphic temperature peak. Here, we characterise the shape of *PT* paths through the rate of pressure change at the temperature maximum, $dP/dt|_{Tmax}$. In correspondence with the well-used terms "clockwise" and "anticlockwise", we term this parameter the clockwiseness of a *PT* path, C. C is not only a very simple description of shape, but it is also a useful measure of the total duration of a given pressure at the temperature peak, T_{max}, which may be valuable information for the kinetic interpretation of pressure sensitive mineral equilibria. Using this description "clockwise" paths are those with negative C while "anticlockwise" paths are

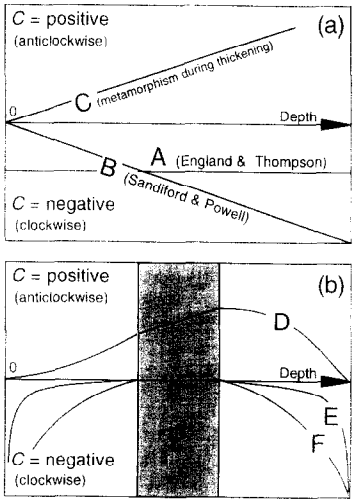

Fig. 1. Schematic illustration of the clockwiseness of *PT* paths, C, as a function of depth for a range of common metamorphic environments. (a) Three simple models of conductive metamorphism; (A) is for the model of England and Thompson (1984); (B) is for the model of Sandiford and Powell (1986); (C) is for metamorphism during ongoing convergent deformation; (b) illustrates more complicated interrelationships for contact metamorphism around a sill-shaped intrusion in the middle crust (shaded area), accompanied by a waning deformation; (D) is the pressure changes of the lithostatic pressure component; (E) and (F) represent the pressure changes of the deviatoric stress component to the pressure field, τ, for the same model as (D) for slow and fast initial deformations. All paths are drawn for initial depths of material points.

those with positive C and isobaric cooling paths are characterised by $C = 0$. It should be pointed out that there are cases where this description may be misleading as large positive C at T_{max} may last only for small absolute P-intervals and may be followed by negative pressure changes. In Fig. 1(a) we have plotted C against depth in the crust for a range of common tectonic settings. Curve A is for the model of England and Richardson (1977) and England and Thompson (1984) where a time-invariant erosion rate at the surface induces decompression during the thermal relaxation of a previously thickened crust. Therefore, independent of the time of T_{max}, the decompression rate remains constant (negative but constant C). In contrast, *PT* paths that form during homogeneous thickening or thinning of

the crust are characterised by increasing C with depth (curves B and C). Curve B corresponds to the metamorphic model of Sandiford and Powell (1986). Curve C corresponds to a metamorphic environment where the heating–cooling cycle occurs during ongoing convergent deformation.

The large shape differences of the curves in Fig. 1(a) suggest that the parameter C may be a useful function that allows to interpret the nature of a metamorphic setting if it can be measured across a metamorphic terrain. However, the models illustrated by curves A, B and C are rather simplistic views of metamorphism. For example, the clockwiseness C for curves B and C increases linearly with depth only if the crust deforms homogeneously. More complicated interrelationships between deformation and metamorphism must occur in deforming rock piles (Fig. 1(b)) and some of those have been modelled by Sandiford et al. (1991) and Stüwe et al. (1993). For example, curve D (Fig. 1(b)) corresponds to the lithostatic pressure change in convergent orogens where the vertical strain rate, $\dot{\epsilon}_t$, decreases with time. Because $\dot{\epsilon}_t$ is time dependent, the shape of D in this model depends on the time of the metamorphic peak, $t_{T\max}$ with respect to the stage in the deformation history and C cannot be plotted on the basis of the strain-rate model alone as has been done for the models shown in Fig. 1(a). For curve D a sill-shaped model intrusion is assumed to occupy midcrustal levels as represented by the shaded area in the centre of the plot. The time of the contact-metamorphic peak that is the consequence of this magma emplacement increases with distance form the intrusion (Jaeger, 1964). Therefore, C must decrease with distance from the intrusion because strain rate also decreases after intrusion. C comes to zero at the margins of the plot only because the deformation history used to calculate curve D was assumed to terminate at a time when the margin of the plot reach their metamorphic temperature peak. Curves E and F illustrate the deviatoric stress contribution to the pressure field, τ_z, for the same model assumptions as D assuming a rheology which can support temperature and stain-rate dependent stresses (see below). Curve E is for a slow initial strain rate, curve F is for a fast initial strain rate. Their difference is because of the strain-rate dependence of τ_z with slower strain rates implying lower stresses. The decrease in C of E and F with distance from the intrusion is the consequence of lower $T_{\max}$ at larger distances coupled with the exponential temperature dependence of τ_z. In order to explain the relationships causing the shape of curves D, E and F we will now focus on a more detailed evaluation of the variation of C for the model that describes curves D, E and F.

3. An analytical description of clockwiseness, C

In order to illustrate the components of PT paths that may arise in actual deforming mountain belts with temperature-sensitive rheologies we develop approximate analytical descriptions for PT paths using descriptions for both the temperature and the pressure field as a function of time and depth. In order to do so we follow the approach of Stüwe and Sandiford (1994) assuming a simple one-dimensional model-crust and a model in which the temperature evolution is influenced by the emplacement and cooling of magmatic heat source and the strain-rate evolution is superimposed externally. We assume that the model-crust deforms homogeneously with no vertical strain-rate gradients and that the bulk strain rate is determined by some lithospheric scale force balance.

3.1. The pressure field

We assume an environment of horizontal biaxial compression. Then, the principal stresses of a one-dimensionally deforming column may be given by the horizontal, σ_{xx}, and vertical, σ_{zz}, stresses ($\sigma_{xx} > \sigma_{zz}$). We describe pressure, $P(z)$, at depth z in terms of the lithostatic stress contribution $P_{\text{lith}} = \sigma_{zz}$, and the deviatoric stress contribution which we assume to be

$$P_{\text{dev}} = \tau_z = \frac{\sigma_{xx} - \sigma_{zz}}{2}$$

so that

$$P(z) = P_{\text{lith}} + P_{\text{dev}} = \sigma_{zz} + \tau_z = g\int_h^z \rho_z dz + \tau_z \quad (1)$$

where g is the gravitational acceleration and ρ_z is the density distribution with depth. If the density is assumed to be independent of depth, P_{lith} of Eq. (1) as a function of time, t, is given by

$$P_{\text{lith}} = \sigma_{zz} = \rho g z + \rho g z \left(1 + \int_0^t \dot{\epsilon}_t \mathrm{d}t\right) = \rho g z (\epsilon_t + 1) \tag{2}$$

where $\dot{\epsilon}_t$ is the vertical strain rate as a function of time, ϵ_t is the thickening strain at time t and z is the depth of the rock prior to deformation. The deviatoric component τ_z is a function of the deformation mechanism. We assume a power law rheology so that τ_z is a strong function of temperature and strain rate and may be described by

$$P_{\text{dev}} = \tau_z = 0.5 \left(\frac{\dot{\epsilon}_t}{A}\right)^{\frac{1}{n}} \exp\left(\frac{Q}{nRT_z}\right) \tag{3}$$

where A, n and Q are the material constants for power law creep, namely the pre-exponential constant, the power-law exponent and the activation energy, respectively, R is the gas constant, and T_z is the absolute temperature as a function of depth. The total pressure is then given by

$$P_{t,z} = \sigma_{zz} + \tau_z = \rho g z \left(1 + \int_0^t \dot{\epsilon}_t \mathrm{d}t\right) + 0.5 \left(\frac{\dot{\epsilon}_t}{A}\right)^{\frac{1}{n}} \exp\left(\frac{Q}{nRT_z}\right) \tag{4}$$

The pressure history may therefore be uniquely defined by the assumption of a temperature history and assumptions about the strain-rate evolution.

3.2. The temperature field

The temperature evolution is described by the thermal relaxation history of a one-dimensional step-shaped temperature perturbation representing a large sill-shaped intrusion. If the influence of convection and latent heat of fusion is neglected, then the decay of this temperature perturbation may be analytically described by

$$T_{t,z} = T_0 + \frac{T_m - T_0}{2} \left\{ \operatorname{erf}\left[\frac{0.5d - (z - D)}{\sqrt{4\kappa t}}\right] + \operatorname{erf}\left[\frac{0.5d + (z - D)}{\sqrt{4\kappa t}}\right] \right\} \tag{5}$$

where T_0 is the host rock temperature, T_m is the intrusion temperature, d is the thickness of the intrusion, D is its intrusion depth and κ is the thermal diffusivity (Carslaw and Jaeger, 1959). Cooling of this perturbation will result in heating of material points outside the intrusion and this "contact metamorphism" occurs at increasingly later times with distance from the intrusion (Jaeger, 1964; DenTex, 1963). The time of the metamorphic temperature peak, $t_{T\max}$ may be found by differentiating Eq. (5) with respect to time and setting the result to zero to give

$$t_{T\max} = \frac{d(D - z)}{2\kappa \ln\left[-\dfrac{0.5d - (z - D)}{0.5d + (z - D)}\right]} \tag{6}$$

Eqs. (5) and (6) will be used henceforth as a description of the temperature evolution. However, it should be pointed out that many other intrusion geometries may be described analytically. For example, coalescing contact metamorphic aureoles of many intrusions (Barton and Hanson, 1989) superimposed on a realistic geothermal gradient, G, may be described by

$$T_{t,z} = Gz + \frac{T_m - (Gz)}{2} \times \sum_{i=1}^{n} \left\{ \operatorname{erf}\left[\frac{0.5d^i - (z - D^i)}{\sqrt{4\kappa t}}\right] + \operatorname{erf}\left[\frac{0.5d^i + (z - D^i)}{\sqrt{4\kappa t}}\right] \right\} \tag{7}$$

where i is the number of intrusions of magma temperature T_m and d^i and D^i are their respective thicknesses and intrusion depths. Indeed, any polygonal shape for the initial temperature field may be described analytically by appropriate

combination of error function solutions for a temperature step in a semi-infinite half space.

3.3. Strain-rate assumptions

Rather than considering explicitly the orogenic force balance to determine strain rate (e.g. Sandiford et al., 1991), we assume three different strain-rate models, referred to by subscript (I),(II) and (III). The first model is a constant strain rate through time

$$\dot{\epsilon}_{t(\mathrm{I})} = \dot{\epsilon}_{\mathrm{i}} \tag{8}$$

where $\dot{\epsilon}_{\mathrm{i}}$ is the initial strain rate. This scenario is appropriate to an environment where the thermal evolution of a confined intrusion does not depend on the gross lithospheric force balance. The second model describes an exponentially or inverse exponentially decaying strain-rate evolution

$$\dot{\epsilon}_{t(\mathrm{II})} = \dot{\epsilon}_{\mathrm{i}}\left\{1 - \left[\frac{\exp(\alpha t) - 1}{\exp(\alpha t_{\mathrm{f}}) - 1}\right]\right\} \tag{9}$$

where $\dot{\epsilon}_{\mathrm{i}}$ is the strain rate at the time of intrusion, t_{f} is the time where deformation is terminated and α describes the time dependence of the strain rate. Negative α describes exponentially decaying strain rates as in Sandiford et al. (1991, 1992) and positive α describes prolonged deformation after intrusion (Fig. 2). With $\alpha = 0$ Eq. (9) reduces to a linear relation

$$\dot{\epsilon}_{t(\mathrm{II})} = \dot{\epsilon}_{\mathrm{i}}\left(1 - \frac{t}{t_{\mathrm{f}}}\right) \tag{10}$$

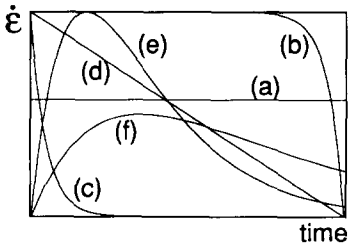

Fig. 2. Schematic illustration of different strain-rate evolutions used in this paper. (a) A constant strain rate through time of model (I). Curves (b), (c) and (d) are of the second model calculated with Eq. (9): (b) is for positive α; (c) is for negative α; and (d) is the linear relationship for $\alpha = 0$ described by Eq. (10). Curves (e) and (f) are calculated for model (III) with Eq. (11). Both curves are for the same total strain but different $\dot{\epsilon}_{\mathrm{i}}$ and $t_{\dot{\epsilon}\mathrm{i}}$.

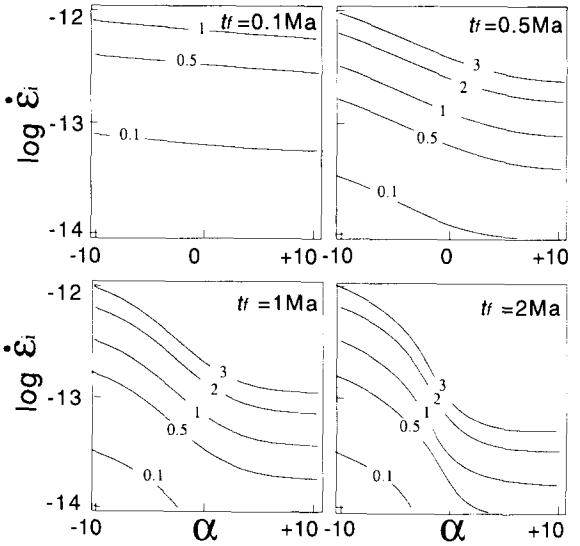

Fig. 3. Model (II) The maximum strain rate, $\dot{\epsilon}_{\mathrm{i}}$, against the exponential drop-off parameter α contoured for total strain for four different total deformation times, t_{f} calculated with Eq. (17).

This second strain-rate model corresponds to a scenario in which deformation is initiated by the intrusion of a heat source and only decays during the cooling of the heat source and contact metamorphism. As a third model we assume the strain-rate evolution

$$\dot{\epsilon}_{t(\mathrm{III})} = \dot{\epsilon}_{\mathrm{i}}\left(\frac{t}{t_{\dot{\epsilon}\mathrm{i}}}\right)\exp\left(1 - \frac{t}{t_{\dot{\epsilon}\mathrm{i}}}\right) \tag{11}$$

in which $\dot{\epsilon}_{\mathrm{i}}$ is also the maximum strain rate which occurs here not at the time of intrusion but occurs at time $t_{\dot{\epsilon}_{\mathrm{i}}}$ a short time thereafter (Fig. 2). This strain-rate history starts at zero and describes an environment where deformation commences owing to intrusion. The second and third model were also explored by Stüwe and Sandiford (1994). One advantage of these two models is that the parameters describing their shape ($\dot{\epsilon}_{\mathrm{i}}$, t_{f} and α for model (II) and $t_{\dot{\epsilon}_{\mathrm{i}}}$ and $\dot{\epsilon}_{\mathrm{i}}$ for model (III)) are dependent when the total strain is prescribed (Figs. 3 and 4). The second model is particularly flexible because it also allows an arbitrary choice of t_{f} as the coupling of $\dot{\epsilon}_{\mathrm{i}}$ and α prescribes deformation histories that are quite robust for a large range of t_{f}. Here we explore

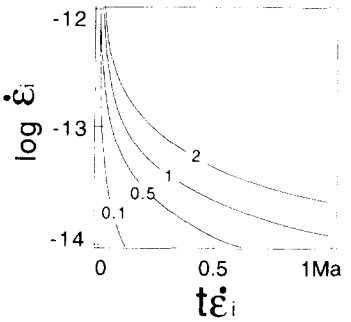

Fig. 4. Model (III) The maximum strain rate, $\dot{\epsilon}_i$, against the time of the maximum strain rate $t_{\dot{\epsilon}i}$ contoured for total strain thickening strain calculated with Eq. (18).

deformation histories that last for about twice the time of the thermal time constant of the intrusion so that

$$t_f = 2\frac{d^2}{\kappa}$$

This number is roughly consistent with the deformation histories of Sandiford et al. (1991). The strains at any time step during the deformation history are given for the first model by

$$\epsilon_{t(I)} = \int_0^t \dot{\epsilon}_t \mathrm{d}t = \dot{\epsilon}_i t \tag{12}$$

For the second model strain rate they are given by

$$\epsilon_{t(II)} = \int_0^t \dot{\epsilon}_t \mathrm{d}t = \dot{\epsilon}_i \left\{ \frac{1 - \exp(\alpha t) + \exp(\alpha t_f)\alpha t}{\alpha[\exp(\alpha t_f) - 1]} \right\} \tag{13}$$

For computational implementation of Eq. (13), time is better expressed in millions of years. Then, Eq. (13) may be rewritten as

$$\epsilon_{t(II)} = \int_0^t \dot{\epsilon}_t \mathrm{d}t = \dot{\epsilon}_i \left\{ \frac{m - m\exp(\alpha t/m) + \exp(\alpha t_f/m)\alpha t}{\alpha[\exp(\alpha t_f/m) - 1]} \right\}$$

where $m = 3.15 \times 10^{13}$ s and time is in millions of years. The strain for the third model evolution is given by

$$\epsilon_{t(III)} = \int_0^t \dot{\epsilon}_t \mathrm{d}t = \dot{\epsilon}_i t_{\dot{\epsilon}i} \exp\left[1 - \frac{1 + (t/t_{\dot{\epsilon}i})}{\exp(t/t_{\dot{\epsilon}i})}\right] \tag{14}$$

For the third model the thickening strain that has occurred prior to $t_{\dot{\epsilon}i}$ is given by

$$\epsilon_{t=t\dot{\epsilon}i}(\mathrm{III}) = \int_0^{t_{\epsilon i}} \dot{\epsilon}_t \mathrm{d}t = \dot{\epsilon}_i t_{\dot{\epsilon}i}[\exp(1) - 2] \tag{15}$$

The total strains integrated until the end of deformation are given for the first model by

$$\epsilon_{\mathrm{tot(I)}} = \int_0^{t_f} \dot{\epsilon}_t \mathrm{d}t = \dot{\epsilon}_i t_f \tag{16}$$

For the second model it is given by

$$\epsilon_{\mathrm{tot(II)}} = \int_0^{t_f} \dot{\epsilon}_t \mathrm{d}t = \dot{\epsilon}_i \left\{ \frac{1 + \exp(\alpha t_f) \cdot (\alpha t_f - 1)}{\alpha[\exp(\alpha t_f) - 1]} \right\} \tag{17}$$

or, if the times are in million years

$$\epsilon_{\mathrm{tot(II)}} = \int_0^{t_f} \dot{\epsilon}_t \mathrm{d}t = \dot{\epsilon}_i \left\{ \frac{m + \exp(\alpha t_f/m)(\alpha t_f - m)}{\alpha[\exp(\alpha t_f/m) - 1]} \right\}$$

For model (III) the total strain is only reached after infinite time and is given by

$$\epsilon_{\mathrm{tot(III)}} = \int_0^{\infty} \dot{\epsilon}_t \mathrm{d}t = \dot{\epsilon}_i t_{\dot{\epsilon}i} \exp(1) \tag{18}$$

These relationships may now be substituted into the equations given for the pressure and temperature field.

3.4. PT path calculation

Eqs. (1)–(18) were implemented in the software MATHEMATICA as parametric plotting routines so that temperatures and pressures, both as a function of time may be plotted as continuous *PT* paths. However, for the most simple form of the temperature field of Eq. (5) it is possible to derive a direct expression for the clockwiseness, *C*. The pressure change at any point of a *PT* path is obtained by differentiating the lithostatic

and the deviatoric components with respect to time and adding so that

$$C = \frac{dP_{tot}}{dt} = \frac{dP_{lith}}{dt} + \frac{dP_{dev}}{dt} \quad (19)$$

where the lithostatic contribution to the pressure change for all models is given by

$$\frac{dP_{lith}}{dt} = \rho g z \dot{\epsilon}_t \quad (20)$$

and the deviatoric contribution to the pressure change is given for all models by

$$\frac{dP_{dev}}{dt} = \gamma - \tau_{t,z}\left(\frac{\beta Q}{nRT^2}\right) \quad (21)$$

where β is given by

$$\beta = \frac{dT}{dt} = \frac{(T_m - T_0)}{2} \times \left(- \frac{0.5d - (z - D)}{2\exp\left\{\frac{[0.5d - (z-D)]^2}{4\kappa t}\right\}\sqrt{\pi\kappa t^3}} - \frac{0.5d + (z - D)}{2\exp\left\{\frac{[0.5d + (z-D)]^2}{4\kappa t}\right\}\sqrt{\pi\kappa t^3}} \right)$$

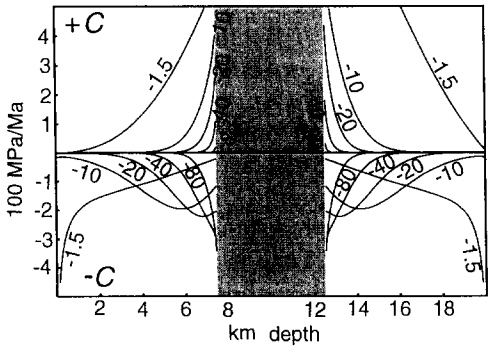

Fig. 5. C plotted against depth in the crust for a constant background temperature of 400°, intrusion temperature of 800° where the intrusion occupies the shaded area of the plot. For this plot, strain-rate model (II) was used and C_{dev} and C_{lith} are plotted separately. The contributions of C_{dev} are the curves with negative C, the contributions of C_{lith} are the curves with positive C. The strain-rate history parameters are $\dot{\epsilon}_i = 10^{-13}\ s^{-1}$ and $t_f = 1$ Ma. Contours are for α.

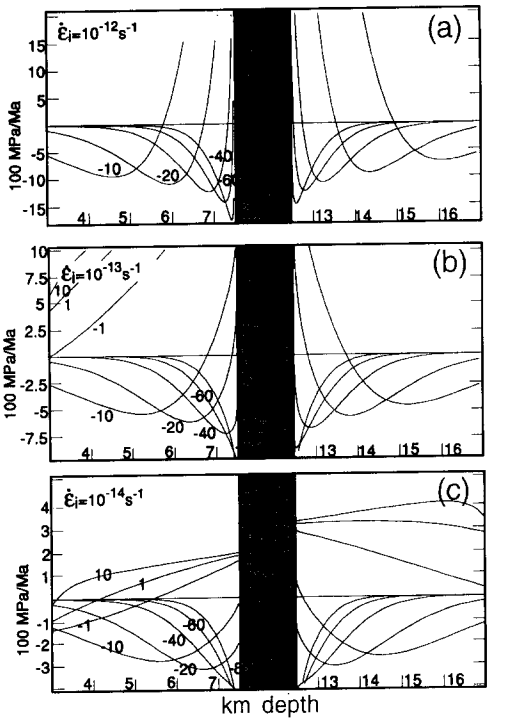

Fig. 6. C plotted against depth in the crust for $T_0 = 400°$ and $T_m = 800°$ where the intrusion occupies the shaded area of the plot. The plot is for strain-rate model (II) and a range of $\dot{\epsilon}_i$ with $t_f = 1$ Ma and contoured for α. (b) Corresponds to Fig. 5. The asymmetry of the curves with respect to the intrusion is a function of the larger contribution of the lithostatic pressure component at greater depths. Note that the intrusion (shaded area) is shown narrower than actual so that the depth axis missed 3 km in the centre.

and where γ is given by

$$\gamma_{(I)} = 0$$

$$\gamma_{(II)} = \tau_{t,z}\left\{ - \frac{\exp(\alpha t)\alpha\dot{\epsilon}_i}{\dot{\epsilon}_t n[\exp(\alpha t f) - 1]} \right\} = \tau_{t,z}\left\{ - \frac{\exp(\alpha t/m)\alpha\dot{\epsilon}_i}{m\dot{\epsilon}_t n[\exp(\alpha t f/m) - 1]} \right\}$$

$$\gamma_{(III)} = \tau_{t,z}\left(\frac{t_{\dot{\epsilon}i} - t}{t_{\dot{\epsilon}i} n t}\right)$$

If the time of the metamorphic temperature peak, $t_{T\max}$, is substituted from Eq. (6) into Eq.

(21) then $\beta = 0$ and the total pressure change at the temperature maximum is

$$C = \rho g z \dot{\epsilon}_t + \gamma \qquad (22)$$

in which $\rho g z \dot{\epsilon}_t$ describes the lithostatic pressure change due to burial (always positive for thickening models) and the γ describes the deviatoric pressure changes (always negative for decreasing strain-rate evolution at the temperature peak where $\beta = 0$).

4. Some results of the model calculations

To illustrate the complexities of *PT* paths we have evaluated Eq. (22) for the clockwiseness of *PT* paths for a range of parameters, in particular for different deformation histories. For the rheological parameters we use $Q = 2.5 \times 10^5$ J mol^{-1}, $n = 3$ and $A = 2 \times 10^{-4}$. These rheological data allow rocks to sustain deviatoric stresses of the order of 100 MPa at 400°–500° and geologically realistic strain rates. For a discussion and justification of these parameters we refer the interested reader to our parallel study (Stüwe and Sandiford, 1994). As other constants we use $\rho = 2700$ kg m^{-3} for the density of the crust, $\kappa = 10^{-6}$ m^2 s^{-1} for the thermal diffusivity, $R = 8.314$ J mol^{-1} K^{-1} for the gas constant and $g = 9.81$ m s^{-2} for the gravitational acceleration. If not stated otherwise we use for the temperature field an initial thickness of the one-dimensional sill of $d = 5$ km, an intrusion depth $D = 10$ km, a background temperature $T_0 = 400°$ and an intrusion temperature of $T_m = 800°$. Fig. 5 shows C for these parameters and for the second strain-rate model using $\dot{\epsilon}_i = 10^{-13}$ s^{-1} and a total time of deformation of $t_f = 1$ Ma. C_{lith} and C_{dev} are plotted separately. The contours are for different α. The negative pressure changes are due to the decay of the deviatoric stress field and are of the same magnitude but different sign as the lithostatic pressure changes owing to continued burial. In Fig. 6 C_{tot} is shown for a range of deformation histories characterised by $t_f = 1$ Ma and $\dot{\epsilon}_i = 10^{-12}$ s^{-1} (Fig. 6(a)), $\dot{\epsilon}_i = 10^{-13}$ s^{-1} (Fig. 6(b)) and $\dot{\epsilon}_i = 10^{-14}$ s^{-1} (Fig. 6(c)). The total strains implied by each calculation may be derived from

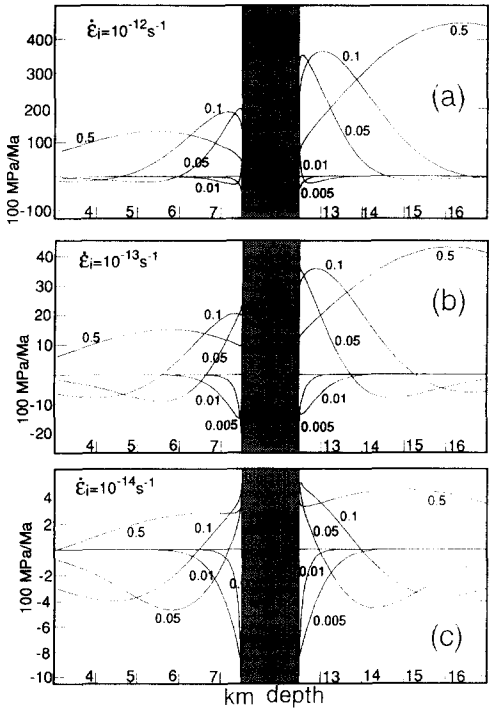

Fig. 7. C plotted against depth in the crust for $T_0 = 400°$ and $T_m = 800°$ where the intrusion occupies the shaded area of the plot. The plot is for strain-rate model (III), a range of $\dot{\epsilon}_i$ and contoured for $t_{\dot{\epsilon}i}$. Note that, in contrast to Fig. 6, C increases initially with distance from the intrusion because the strain rate increases in time as well.

Fig. 3. The clockwiseness of the third model is evaluated in Fig. 7 for the same range of maximum strain rates and contoured for $t_{\dot{\epsilon}i}$.

The curves in Figs. 5, 6 and 7 connect C through depth and time and correspond, therefore, to piezothermal arrays as defined by England and Thompson (1984). Along each curve time increases with distance from the intrusion as given by Eq. (6). Time is zero at the contact and increases rapidly towards the margins of the plots. Below, we concentrate our discussion of the results using Fig. 6 as an example. At the onset of the evolution, lithostatic pressure changes are extremely large (Eq. 20) and outweigh the changes of τ (Eq. 21), which are small at high temperatures despite the large strain-rate changes. At larger distances from the intrusion both, the changes of P_{lith} and those of τ decrease owing to

the assumed decay of strain rate. However, because of the much lower peak temperatures at larger distance (Eqs. 5 and 6) the changes of τ become relatively much more significant. For large negative α the deformation history is concentrated at a short time after intrusion so that the strain-rate changes are extremely large at high T_{max} so that this coupling of P_{lith} and τ changes is dominated by the deviatoric component and C is negative. For larger α (-1 to $+10$) many of the strain-rate changes occur at later times so that the lithostatic component dominates. For intermediate deformation histories ($\alpha = -10$ to -20 at $\dot{\epsilon}_i \approx 10^{-13}$ s^{-1}) the increasing relative importance of changes of τ with time and distance is largely balanced by the decreasing importance of changes of P_{lith} so that a transition from clockwise to anticlockwise paths occurs at a discrete distance from the intrusion. These features are robust towards changes of t_f and d. In fact, for $t_f = 2$ Ma the diagram is practically identical as the important strain-rate changes still occur in the first part of the evolution, whilst for $t_f = 0.5$ Ma much of the evolution shown in Fig. 6 becomes compressed into a small region around the intrusion. An equivalent effect occurs for smaller intrusions and for larger emplacement depths the lithostatic component becomes relatively more important. This may also be seen in the asymmetry of the curves in Figs. 5 and 7 above and below the intrusion.

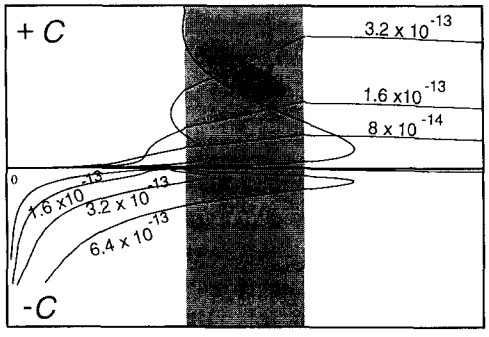

Fig. 8. C plotted against depth in the depth of rocks at the time of the metamorphic peak t_{Tmax}. Lithostatic and deviatoric stress changes are plotted separately. Curves with negative C values are for the deviatoric component C_{dev}, curves with positive values are for the lithostatic component C_{lith}. The curves correspond to curves (D), (E) and (F) in Fig. 1 for a range of initial strain rates.

An interesting result is that all deformation histories for which a qualitative change of the shape of PT paths occurs at a significant distance from the intrusion, correspond to total strains of the order of 0.1–0.5 (Fig. 3). Such strains are consistent with other models describing the LPHT metamorphic environment (e.g. Stüwe et al., 1993). The clockwiseness corresponding to the third strain-rate model (Fig. 7) bears the same features as discussed above with the difference that strain-rate changes are initially positive. Therefore, only positive pressure changes occur early and near the intrusion whilst the later part of the evolution is similar to that shown in Fig. 6.

5. Discussion

The results presented in the last section show that metamorphic PT paths may vary from clockwise to anticlockwise merely as a function of distance from a transient heat source such as a sill-shaped intrusion. This result may have important implications for the interpretation of PT paths and has been discussed by Stüwe and Sandiford (1994). Our aim has been to illustrate the complexities that may develop in PT paths given the feedback between a temperature sensitive rheology and a thermal evolution appropriate to orogenic belts. These complexities are readily portrayed in the C–z diagram. However, these diagrams hide two critical pieces of information.

(1) Figs. 5,6 and 7 are plots of C for initial depths and not for peak depths or pressures. Plotting C for the depth and the time of the temperature peak will distort the diagrams in a depth- and time-proportional fashion towards depth (Fig. 8). Material points near the intrusion will experience their metamorphic peak very early so that the peak depth will be little different from the initial depth. Material points near the surface will also undergo little depth change during thickening deformation, independent of the time of their metamorphic peak. However, the peak depths of most rocks will increase with distance from the intrusion as the metamorphic peak oc-

curs at later times. This will be superimposed on the linear depth increase owing to initial depth. In Fig. 8 curves (D), (E) and (F) from Fig. 1 are re-plotted for peak depths of the rocks as calculated with Eq. (6) and Eq. (13) substituted into Eq. (2) and are shown for a range of strain rates. It may be seen that different rocks pass through the same depth at their metamorphic peak because they experience T_{max} at different times.

(2) Plots of C hide pressure changes at any finite time after the temperature peak. Indeed, in Eq. (21) β, and therefore the entire second term, become zero at $t_{T\max}$. The deviatoric contribution to C is therefore only a function of the strain-rate changes at T_{max}. During subsequent cooling β is finite and there will be positive τ changes owing to temperature decrease interplaying with negative τ changes owing to strain-rate decrease (see Eq. 3). In order to evaluate absolute pressure changes, a finite integration of Eq. (20) and Eq. (21) may be performed. In Fig. 9 we illustrate the finite pressure changes after 20% of the temperature change of the cooling history has occurred. A comparison of Figs. 9(a) and (b) shows that the finite pressure changes per 20% of the cooling interval are similar to those of the pressure change rate at T_{max}.

5.1. Geological implications

The thermal model used in this paper has been used extensively to describe features of the LPHT metamorphic environment (e.g. Lux et al., 1986; DeYoreo, 1989; Sandiford et al., 1991, 1992; Stüwe and Sandiford, 1994). However, this model is extremely schematic and detailed application of the shape of the *PT* paths presented in this paper to real terrains is impossible. However, the principal result, namely that the clockwiseness of *PT* paths may change dramatically across a high-grade terrain, has some fundamental implications for the interpretation of metamorphic *PT* paths of LPHT terrains. It challenges the widely accepted notion that *PT* paths may be used to infer depth changes of rocks. As this result is strongly dependent on the pressure contribution of the deviatoric stress field it depends on the assumption of the rheological parameters — a data set

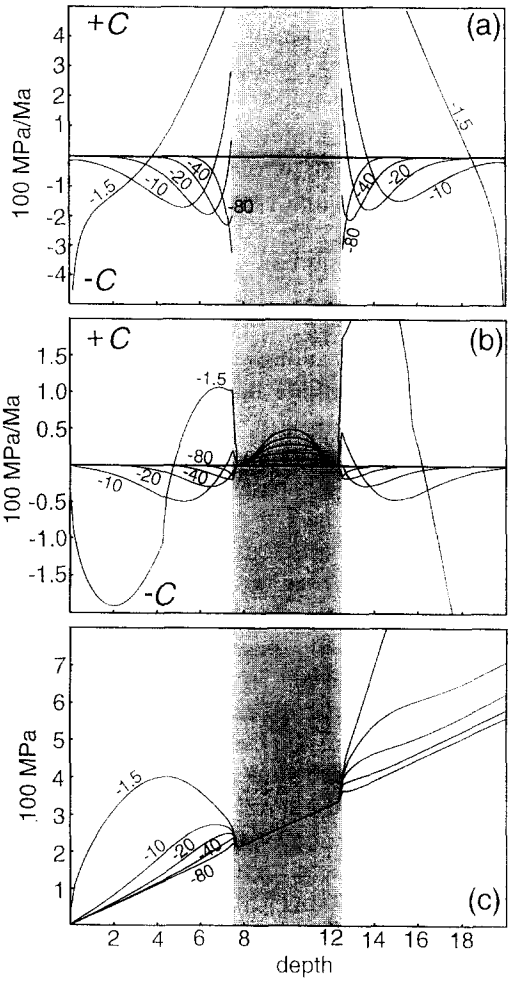

Fig. 9. (a) C plotted against initial depth of rocks for the same parameters as Figs. 5 and 6(b); (b) finite pressure changes over the first 20% of the cooling history; (c) peak pressures against initial depths of rocks.

which remains highly contentious. Here we have assumed a rheology which allows support of up to about 100 MPa at 400° and geologically reasonable strain rates. This is consistent with field and experimental evidence (Brace and Kohlstedt, 1980; Molnar and England, 1990; Molnar, 1993). Pressure changes caused by these assumptions are comparable to those observed in many LPHT terrains indicating that such *PT* paths may not need to be interpreted as the consequence of tectonically induced depth changes.

6. Conclusion

This study has shown that the clockwiseness of *PT* paths recorded in profiles across high-grade terrains may be a useful parameter to interpret their tectonic setting. In LPHT terrains, such paths may vary from clockwise to anticlockwise as a reflection of the interplay of rapid changes of the deviatoric and lithostatic components of the pressure field. The distance from a heat source at which the transition from clockwise to anticlockwise *PT* paths occurs is a function of the relative duration of deformation and cooling history. It is therefore suggested that the widespread record of clockwise paths in many LPHT terrains may rather bear information on the time scale of deformation, than about the exhumation history of the terrains.

Acknowledgements

This manuscript has profited from extensive discussions with S. Zhou, D. Coblentz and R. Powell. T. Will is thanked for help with the graphics output of some of the figures.

References

Barton, M.D. and Hanson, R.B., 1989. Magmatism and the development of low pressure metamorphic belts: Implications from the western United States and thermal modelling. Geol. Soc. Am. Bull., 101: 1051–1065.

Brace, W.F. and Kohlstedt, D.L., 1980. Limits on lithospheric stress imposed by laboratory experiments. J. Geophys. Res., 85: 6248–6252.

Carslaw, H.S. and Jaeger, J.C., 1959. Conduction of Heat in Solids. Oxford Science, Oxford.

denTex, E., 1963. A commentary on the correlation of metamorphism and deformation in space and time. Geol. Mijnbouw, 42: 170–176.

DeYoreo, J.J., Lux, D.R.T., Guidotti, C.V., Decker, E.R. and Osberg, P.H., 1989. The Acadian history of western Maine. J. Metamorphic Geol., 7: 169–190.

England, P.C. and Richardson, S.W., 1977. The influence of erosion upon the mineral facies of rocks from different metamorphic environments. J. Geol. Soc., London, 134: 201–213.

England, P.C. and Thompson, A.B., 1984. Pressure temperature time paths of regional metamorphism I. Heat transfer during the evolution of regions of thickened continental crust. J. Petrol., 25: 894–928.

Harley, S.L., 1989. The origin of granulites: a metamorphic perspective. Geol. Mag., 126: 215–247.

Jaeger, J.C., 1964. Thermal effects of intrusions. Rev. Geophys., 2: 443–466.

Lux, D.R., DeYoreo, J.J., Guidotti, C.V. and Decker, E.R., 1986. Role of plutonism in low pressure metamorphic belt formation. Nature, 323: 794–796.

Mancktelow, N., 1993. Tectonic overpressure in competent mafic layers and the development of isolated eclogites. J. Metamorphic Geology, 11: 801–812.

Molnar, P., 1993. Brace Goetze Strength profiles, the partitioning of strike-slip and thrust faulting at zones of oblique convergence, and the shear-heat flow paradox on the San Andreas Fault. In: B.Evans and T.F. Wong (Editors), Fault Mechanics and Transport Properties of Rocks: A Festschrift in Honour of W.F.Brace. Academic, London, pp. 124–142.

Molnar, P. and England, P., 1990. Temperature, heat flux and frictional stress near major thrust faults. J. Geophys. Res., 95: 4833–4856.

Sandiford, M. and Powell, R., 1986. Deep crustal metamorphism during continental extension; modern and ancient examples. Earth Planet. Sci. Lett., 79: 151–158.

Sandiford, M., Martin, N., Zhou, Z. and Fraser, G., 1991. Mechanical consequences of granite emplacement during high-T, low-P metamorphism and the origin of "anticlockwise" PT paths. Earth Planet. Sci. Lett., 107: 164–172.

Sandiford, M., Foden, J., Zhou, S. and Turner, S., 1992. Granite genesis and the mechanics of convergent orogenic belts with application to the southern Adelaide Fold belt. Trans. R. Soc. Edinburgh, Earth Sci., 83: 83–93.

Sisson, V.B. and Hollister, L.S., 1988. Low pressure facies series metamorphism in an accretionary sedimentary prism, southern Alaska. Geology, 16: 358–361.

Sisson, V.B., Hollister, L.S. and Onstott, T.C., 1989. Petrologic and age constraints on the origin of a low pressure/high temperature metamorphic complex, southern Alaska. J. Geophys. Res., 94: 4392–4410.

Stüwe, K. and Sandiford, M. 1994. Contribution of deviatoric stresses to metamorphic P–T paths: an example appropriate to low-P, high-T metamorphism. J. Metamorphic Geol., 12: 445–454.

Stüwe, K., Sandiford, M. and Powell, R., 1993. Episodic metamorphism and deformation in low pressure high temperature terrains. Geology, 21: 829–832.

Yamamoto, H., 1992. Contrasting metamorphic P–T–time paths of Kohistan granulites and tectonics of the western Himalayas. Abst. II-6-2 P-22-2256, 29th International Geological Congress, Kyoto Abs. Vol. 2, p. 428.